SPH Simulation of Earthquake-induced Slope Failure

Y. Ono
Tottori University, Japan

SUMMARY:
The Smoothed Particle Hydrodynamics (SPH) method for simulation of earthquake induced slope failure is presented. The SPH method was first invented for simulating dynamic behavior of compressive viscous fluid in the late 1970s and has been applied to other various problems in engineering field. So far the SPH method has been extended to handle not only fluid dynamics but also solid dynamics. The most advantage of the SPH method compared to other well established numerical method, such as the Finite Element Method, the Finite Discrete Method et al., is feasibility of analyzing discontinuity problem. This feature of the SPH method is desirable to earthquake induced slope failure simulation because slope failure phenomena posses discontinuity inherently. In this paper, the SPH method is adapted to simulate the earthquake induced slope failure. The SPH method can describe full dynamic behavior of a slope excited by earthquake and possible to predict the final configuration of slope after failure.

Keywords: Numerical method, Smoothed particle hydrodynamics, Slope failure, Earthquake response

1. INTRODUCTION

Slope failures often give serious damages to the lifeline systems. For instance, the external power supply system of Fukushima Dai-ichi Nuclear Power Station suffered severe damages caused by slope failure following the 2011 Tohoku earthquake (NERH, 2011). Numerical simulation is a powerful engineering tool for developing a countermeasures of slope protection against earthquake. The finite element method (FEM) is widely used to assess a slope stability against an earthquake (Toki et al., 1985, Zheng et al., 2005). However, the FEM has some difficulties on the treatment of extremely large discontinuous deformation. Therefore there are some limitations for applying to slope failure problem. The discrete element method (DEM) (Cundall and Struck, 1979) is a popular tool for handling large and discontinuous deformation problem in the geotechnical engineering. However, the DEM has still disadvantages on the determination of its parameters. On the other hand, the smoothed particle hydrodynamics (SPH) method has been developed for handling large deformation problems. Lucy (1977), Gingold and Monaghan (1977) have invented the SPH for simulating viscous fluid flow. Since 1990s, some researchers have extended the method to dynamics of solid bodies (Libersky et al., 1993, Gray et al., 2001). In this study, application of the SPH method to simulation of slope failure during an earthquake are discussed. In the section 2, the concept of the SPH and the fundamental equations are introduced briefly. The analytical model for conducting the SPH simulations is described in the section 3. The results from the SPH simulation and discussions are given in the section 4. Finally the conclusion of this study is summarised in the section 5.

2. SMOOTHED PARTICLE HYDRODYNAMICS

2.1. SPH Formulations

According to the SPH, an approximation form of a function $f(\mathbf{x})$ is given by

$$f(\mathbf{x}) = \int f(\mathbf{x}')W\left(|\mathbf{x}-\mathbf{x}'|, h\right)d\mathbf{x}' \tag{2.1}$$

where $\mathbf{x}$ denotes the position vector and $W\left(|\mathbf{x}-\mathbf{x}'|, h\right)$ is a smoothing kernel function and the cubic-spline kernel (Liu and Liu, 2003) is used in this study. Applying the discretization with particle approximation, the integral in Eqn. 2.1 is rewritten as summation,

$$f(\mathbf{x}^i) = \sum_{j=1}^{N} \frac{m^j}{\rho^j} f(\mathbf{x}^j)W^{ij} \tag{2.2}$$

where $W^{ij} = W\left(|\mathbf{x}^j - \mathbf{x}^i|, h\right)$ and the superscripts *i* and *j* are index of particle and m^i and ρ^j denote the mass and density of particle *i*, respectively. *N* is a number of particles within 2*h* from the particle *i*. The SPH approximation of the spatial derivative of the function $f(\mathbf{x})$ is given by

$$\frac{\partial f\left(\mathbf{x}^i\right)}{\partial x_\alpha} = -\sum_{j=1}^{N} \frac{m^j}{\rho^j} f\left(\mathbf{x}^j\right)\frac{\partial W^{ij}}{\partial x_\alpha} \tag{2.3}$$

where the subscripts α is used to denote the coordinate directions.

The SPH approximating equation of Eqns. 2.2 and 2.3 often suffers from low accuracy due to deficiency of nearby particles. Chen et al. (1999) proposed the Corrective SPH (CSPH) method to prevent the problem. In the CSPH, the SPH Eqns. 2.2 and 2.3 are replaced by

$$f\left(\mathbf{x}^i\right) = \frac{\sum_{j=1}^{N} \frac{m^j}{\rho^j} f(\mathbf{x}^j)W^{ij}}{\sum_{j=1}^{N} \frac{m^j}{\rho^j} W^{ij}} \tag{2.4}$$

and

$$\frac{\partial f\left(\mathbf{x}^i\right)}{\partial x_\alpha} \sum_{j=1}^{N} \frac{m_j}{\rho_j}\left(x_\alpha^j - x_\alpha^i\right)\frac{\partial W^{ij}}{\partial x_\beta} = \sum_{j=1}^{N} \frac{m_j}{\rho_j}\left\{f\left(\mathbf{x}^j\right) - f\left(\mathbf{x}^i\right)\right\}\frac{\partial W^{ij}}{\partial x_\beta} \tag{2.5}$$

respectively. Note that a set of linear equation needs to be solved for each particle in each time step and thus it increases computational costs significantly. In this study, Eqns. 2.4 and 2.5 are used rather than Eqns. 2.2 and 2.3.

2.2. Governing Equations

The equation of motion for a continuum is given by

$$\ddot{u}_\alpha = \frac{1}{\rho}\frac{\partial \sigma_{\alpha\beta}}{\partial x_\beta} + b_\alpha \tag{2.6}$$

where *u* denotes the displacement. ρ and b_α are is the density and the body force respectively. $\sigma_{\alpha\beta}$ is

the stress tensor. Applying Eqn. 2.5 and after several mathematical manipulation (Liu and Liu, 2003), the SPH approximation of Eqn. 2.6 is given by,

$$\ddot{u}_\alpha^i = -\sum_{j=1}^{N} m^j \left(\frac{\sigma_{\alpha\beta}^i}{\left(\rho^i\right)^2} + \frac{\sigma_{\alpha\beta}^j}{\left(\rho^j\right)^2} \right) \frac{\partial W^{ij}}{\partial x_\beta} + b_\alpha^i \tag{2.7}$$

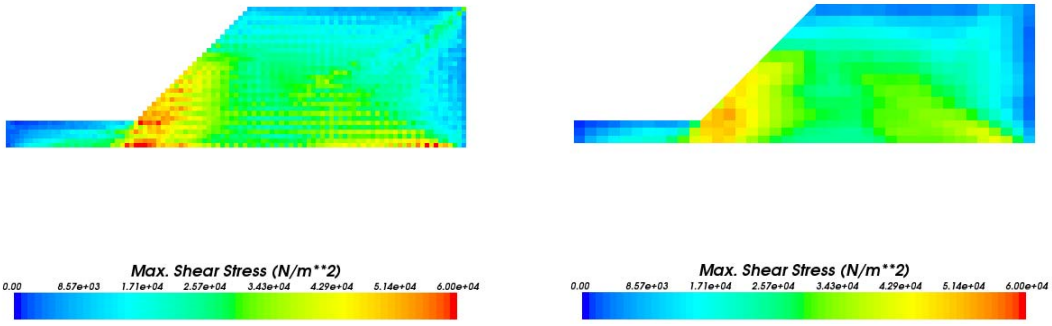

(a) Shear strain distribution by SPH (b) Shear strain distribution by FEM

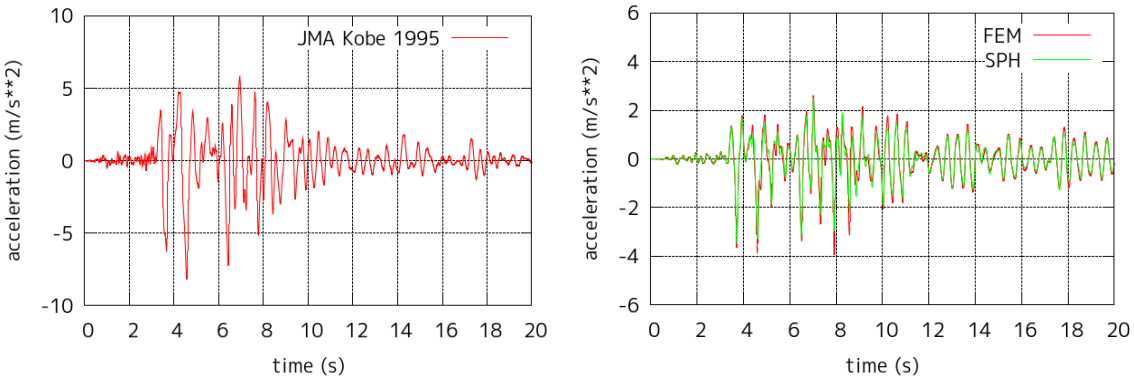

(c) Input ground motion (JMA Kobe 1995) (d) Acceleration response

Figure 1. Validation of the Rayleigh damping

2.3. Rayleigh Damping

The Rayleigh damping is popularly used for the FEM in the earthquake engineering. The Rayleigh damping matrix [*C*] is defined by

$$[C]\{\dot{u}(t)\} = (\alpha_R[M] + \beta_R[K])\{\dot{u}(t)\} \tag{2.8}$$

where [*M*] and [*K*] are the mass matrix and the stiffness matrix respectively. $\{\dot{u}(t)\}$ is the nodal velocity vector at time *t*. α_R and β_R are the damping coefficients. On the other hand, the SPH does not have the mass and the stiffness matrices. Therefore some modifications are required for applying the Rayleigh damping to the SPH simulation. The first order Taylor expansion of the second term of the right-hand side of Eqn. 2.8 gives

$$\beta_R[K]\{\dot{u}(t+\Delta t)\} \approx \beta_R[K]\frac{\{\dot{u}(t+\Delta t)\} - \{\dot{u}(t)\}}{\Delta t} = \beta_R \frac{\{f(t+\Delta t)\} - \{f(t)\}}{\Delta t} \tag{2.9}$$

where $\{f(t)\}$ is the internal force vector and Δt is the time increment. The right-hand side of Eqn. 2.9 is

equivalent to

$$\frac{\beta_R}{\Delta t}\left(\frac{\partial\sigma_{\alpha\beta}(t+\Delta t)}{\partial x_\beta}-\frac{\partial\sigma_{\alpha\beta}(t)}{\partial x_\beta}\right) \tag{2.10}$$

On the other hand, the term $\alpha_R[M]$ in the right-hand side of Eqn. 2.8 corresponds to $\alpha_R\rho$ obviously. Then the Rayleigh damping force for the SPH is given by

$$c_R\cdot\dot{u}_\alpha^i=\left\{\alpha_R\cdot\rho^i+\frac{\beta_R}{\Delta t}\cdot\left(\frac{\partial\sigma_{\alpha\beta}(t+\Delta t)}{\partial x_\beta}-\frac{\partial\sigma_{\alpha\beta}(t)}{\partial x_\beta}\right)\right\}\cdot\dot{u}_\alpha^i \tag{2.11}$$

In Figure 1, the earthquake response of a slope model which calculated by SPH with the 5 % Rayleigh damping is compared with the result from FEM. The shear strain distribution and the response acceleration time history show good agreement each other.

2.4. Artificial Viscosity

Monaghan (1989) introduced the artificial viscosity to prevent unphysical penetration and clumping of particles. The artificial viscosity term is defined by

$$\Pi^{ij}=\frac{-\alpha_\Pi\cdot\left(\frac{c^i+c^j}{2}\right)\cdot\phi^{ij}+\beta_\Pi\cdot\left(\phi^{ij}\right)^2}{\frac{\rho^i+\rho^j}{2}} \tag{2.12}$$

where α_Π and β_Π are the coefficient of the artificial viscosity. *c* is the sound speed and

$$\phi^{ij}=\frac{h^i+h^j}{2}\cdot\frac{\left(\mathbf{v}^j-\mathbf{v}^i\right)\cdot\left(\mathbf{x}^j-\mathbf{x}^i\right)}{\left|\mathbf{x}^j-\mathbf{x}^i\right|^2+\varphi^2} \tag{2.13}$$

where *h* denotes the smoothing length and φ is a parameter inserted to prevent numerical divergence. Introducing the artificial viscosity term, Eqn. 2.7 is replaced by

$$\dot{u}_\alpha^i=-\sum_{j=1}^{N}m^j\left(\frac{\sigma_{\alpha\beta}^i}{\left(\rho^i\right)^2}+\frac{\sigma_{\alpha\beta}^j}{\left(\rho^j\right)^2}+\Pi^{ij}\right)\frac{\partial W^{ij}}{\partial x_\beta} \tag{2.14}$$

2.5. Time Integration

The Leapfrog time integration scheme is used in this study. The velocity and displacement of particle *i* are given by,

$$\dot{u}^i{}_\alpha\left(t+\frac{\Delta t}{2}\right)=\dot{u}^i{}_\alpha\left(t-\frac{\Delta t}{2}\right)+\ddot{u}_\alpha^i(t)\Delta t \tag{2.15}$$

$$u_\alpha^i(t+\Delta t) = u_\alpha^i(t) + \dot{u}_\alpha^i\left(t+\frac{\Delta t}{2}\right)\Delta t \tag{2.16}$$

respectively.

3.SLOPE MODEL

3.1. Model

3.1.1. Geometry and Boundary Condition

In this study, the dynamic behaviour of a slope excited by earthquake is analyzed by using the SPH method. The geometry of the slope model is shown in Figure 2. The rigid boundary condition is given to the bottom of the analytical model. In addition, horizontal component of the displacement is fixed at both of side boundaries.

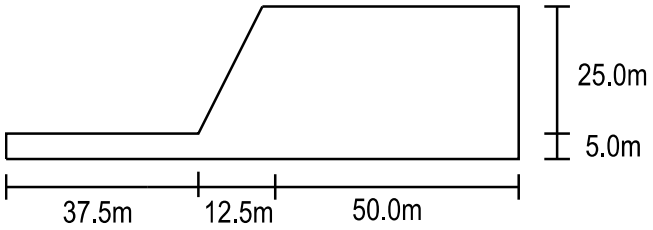

Figure 2. Geometry of slope model

3.1.2. Constitutive Model

The Mohr-Coulomb model is employed for the slope material in this study. According to the Mohr-Coulomb model, the shear strength τ_f is defined by

$$\tau_f = c + \sigma \tan\phi \tag{3.1}$$

where c and ϕ are cohesion and internal friction angle respectively. σ is the normal stress at the state. In addition to the conservative Mohr-Coulomb model, strength drop-off is introduced in this study. For the first failure of the material, the peak cohesion c_p and the peak friction angle ϕ_p are used for Eqn. 3.1. Once the material reached the failure line, the shear strength is dropped off. The residual cohesion c_R and the residual internal friction angle ϕ_R are used for defining the second failure line.

Table 1. Material properties of slope

density ρ	1.61 t/m^3
peak cohesion c_p	143.3 kN/m^2
peak internal friction angle ϕ_p	5.9 deg.
residual cohesion c_R	103.1 kN/m^2
residual internal friction angle ϕ_R	5.9 deg.
elastic modulus E	389000 kN/m^2
Poisson ratio ν	0.466

3.1.3. Initial Particle Arrangement

Three different particle arrangements are used in this study. Particles are regularly arranged with equivalent spacing dp = 0.5, 1.0 and 2.0 m. Figure 3 shows the initial particle arrangements for three cases. Three fixed particle lines are added to the bottom of each model for ensuring the rigid boundary condition. Total number of particles used is shown in the figures.

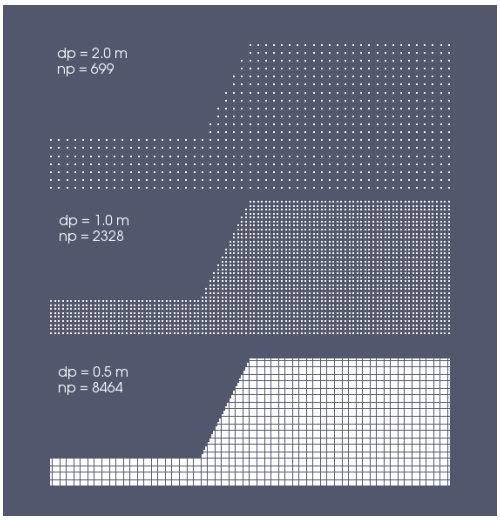

Figure 3. Initial particle arrangement

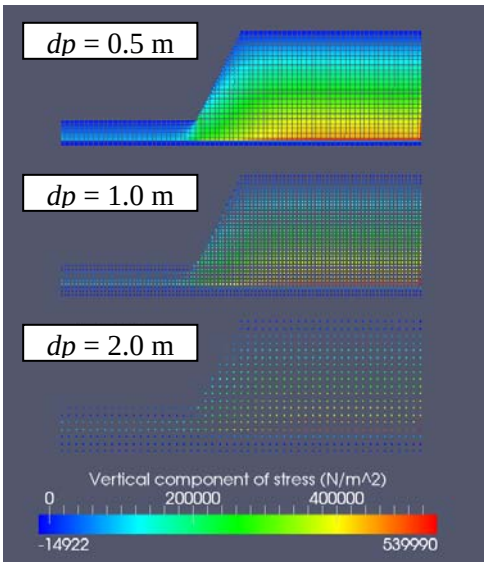

Figure 4. Initial stress distribution obtained by the gravity loading analysis

3.2. Initial Stress Condition

The stress distribution before seismic loading is calculated as the response to the gravity. Initially all stress components are assumed to be zero and then the gravity load is applied gradually to the model. The gravity loading $a(t)$ at the time step t is given by

$$a(t) = \begin{cases} g\sin\left(\dfrac{2\pi}{T}t\right) & 0 \le t < T \\ g & t \ge T \end{cases} \tag{3.2}$$

where g is the acceleration of gravity and T is the duration of loading. In this study, T is fixed to be 5.0s. For the sake of avoiding superfluous vibration during the gravity loading process, an additional damping force $D_\alpha(t)$ is applied.

$$D_\alpha(t) = \frac{\xi}{\Delta t} u_\alpha \tag{3.3}$$

where ξ is a non-dimensional damping coefficient. Bui et al. (2010) recommend that the value should be in range of ξ =0.001 - 0.005. In this paper, the results for ξ =0.005 are presented. Other damping forces, such as Rayleigh damping and artificial damping, are not used here. The distribution of vertical stress component for each case of particle spacing is shown in Figure 4. The initial stress distribution is obtained properly for each size of particle spacing.

3.3. Input Ground Motion

The sinusoidal wave with 1.2 Hz is used for the horizontal component of the input ground motion. The maximum amplitude *A* is set to be 400, 500 and 600 gal. Figure 5 shows the normalized wave form of the motion. In addition, the gravity force is applied to the vertical direction without any other excitation.

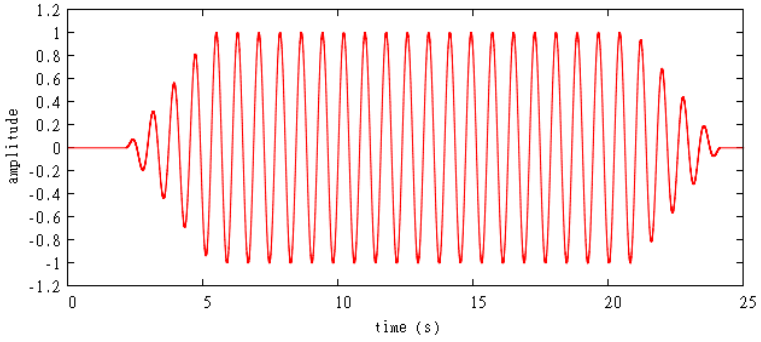

Figure 5. Horizontal input ground motion

4. RESULTS AND DISCUSSIONS

4.1. Response to Ground Motion

The SPH results from different intensity of the input motion are compared in Figure 6. The material properties used here are tabulated in Table 1. Initial particle spacing *dp* is set to be 0.5 m. For artificial viscosity, α_{II} = β_{II} = 0.001 and φ = 0.01 are used. It is observed that failure line appeared from the bottom of the slope and grew up for each case. Slip failure took place and discontinuity appeared at the top of the slop. The displacement of the sliding mass becomes larger depending on intensity of the input motion.

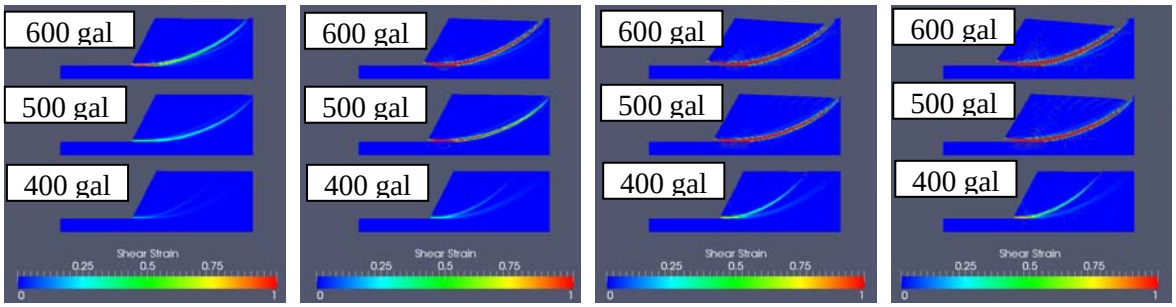

(a) t = 5.0 s (b) t = 10.0 s (c) t = 15.0 s (d) t = 20.0 s

Figure 6. Simulation snapshots (comparison of the intensity of excitation)

4.2. Effect of Particle Density

The effect of the particle density is investigated here. Tree different values of initial particle spacing

are examined; 0.5, 1.0 and 2.0 m. The values of α_{II} = β_{II} = 0.001 and φ = 0.01 are used for the artificial viscosity. The amplitude of the input ground motion is 600 gal. Figure 7 shows the particle configuration at t = 5.0, 10.0, 15.0 and 20.0 s respectively. The failure lines appeared at same location for all cases. However, the width of the slip line and the displacement of the sliding mass are different each other. In general, the smoothing length of the kernel takes larger value when the particle spacing becomes larger. Therefore the larger particle spacing decreases spatial resolution of the simulation.

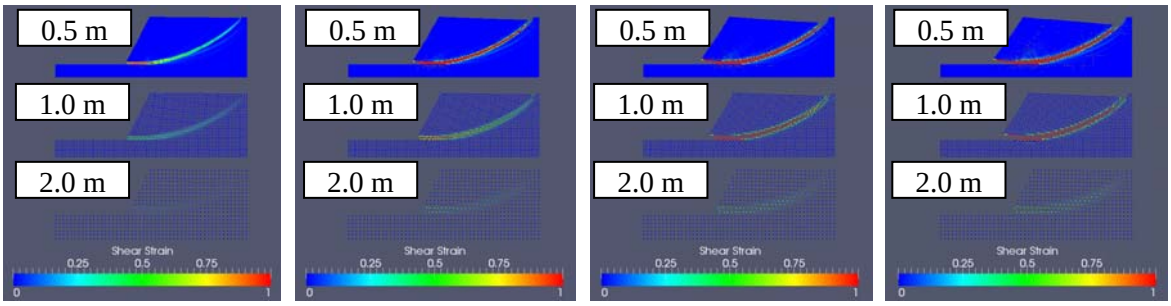

(a) t = 5.0 s (b) t = 10.0 s (c) t = 15.0 s (d) t = 20.0 s

Figure 7. Simulation snapshots (comparison of initial particle spacing)

4.3. Effect of Artificial Viscosity

The artificial viscosity force gives bulk and shear viscosity. In Figure 8, the results are compared for different artificial viscosity parameters. The behaviour of the slope model is quite different though the artificial viscosity is preferred to use for avoiding the unrealistic particle clumping. Therefore the parameters for the artificial viscosity should be chosen carefully.

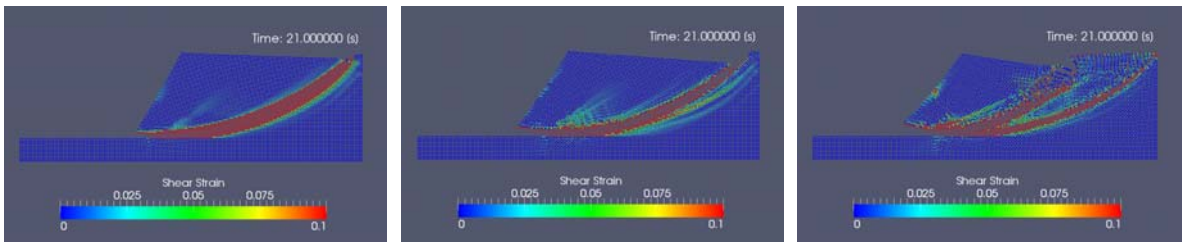

(a) α_{II} = β_{II} = 0.01 (b) α_{II} = β_{II} = 0.001 (c) α_{II} = β_{II} = 0.0001

Figure 8. Simulation snapshots at t = 21.0 s (comparison of artificial viscosity)

4.4. Computational Time

The SPH simulations shown in this paper were carried out on Intel Core i7 3.3GHz CPU and 24GB RAM system. The SPH simulation code used by this study has been developed by the author. The computational times for the cases of dp = 0.5, 1.0, 2.0 m are measured compared in Figure 9. In addition to these cases, the simulation with dp = 0.25 m was carried out though the result is not presented in this paper. The blue solid line is $Cx\log_{10}x$ where x denotes number of particle and C = 1.525E-5. The required computational time can be estimated by using this function. For instance, the SPH simulation with 30,000 particles and 100,000 time steps requires more than two days. More efficient computer code is expected for practical use of the SPH simulation.

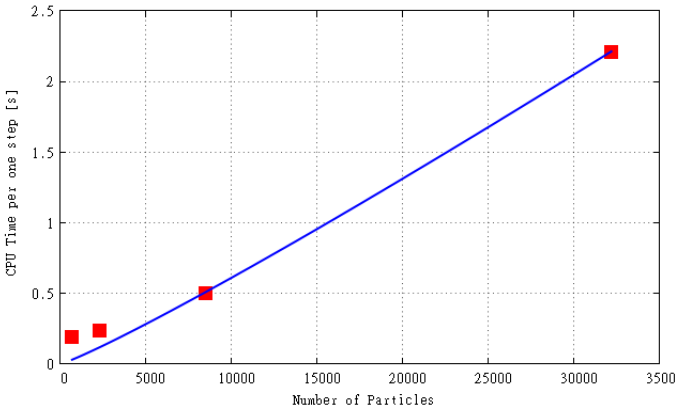

Figure 9. Comparison of elapsed CPU time per one time step

5. CONCLUSIONS

The paper presents the application of the SPH method to simulation of earthquake-induce slope failure. The accuracy of the SPH simulation for the earthquake response analysis is validated by comparison with the FEM method. In addition, the Rayleigh damping force is introduced to SPH. The SPH simulation can represent dynamic behaviour of slope failure including large and discontinuous deformation and can be used to predict the final configuration of the slope after failure. However it is shown that parameters specific to SPH method affect the results and these parameters must be chosen properly. The required CPU cost increases drastically when number of particles used in the simulation increases. Efficient computer code is desired for practical use of the SPH simulation.

AKCNOWLEDGEMENT

This work was supported by the Grant-in-Aid for Young Scientists (B) (23760426) from the Japan Society for the Promotion of Science (JSPS).

REFERENCES

Nuclear Emergency Response Headquaters (2011). Report of Japanese Government to the IAEA Ministerial Conference on Nuclear Safety - The Accident at TEPCO's Fukushima Nuclear Power Stations -.

Toki, K., Miura, H. and Oguni, Y. (1985). Dynamic slope stability analyses with a non-linear finite element method, *Earthquake Engineering and Structural Dynamics*. **13**, 151-171.

Zheng, H., Liu, D.F. and Li, C.G. (2005). Slope stability analysis based on elasto-plastic finite element method. *International Journal of Numerical Methods in Engineering*, **64**, 1871-1888.

Cundall P.A. and Struck, O.D.L. (1979). A discrete numerical model for granular assmblies, *Geotechniquie*, **29**, 47-65.

Lucy, L.B. (1977). Numerical approach to testing the fission hypothesis. *Astronomical Journal*. **82**, 1013-1024.

Ginglold, R.A. and Monaghan, J.J. (1977). Smoothed Particle Hydrodynamics:Theory and Application to Non-spherical stars, *Monthly Notices of the Royal Astronomical Soceiety*. **181**, 375-389.

Libersky, L.D., Petschek, A.G. Carney, T.C. Hipp, J.R. and Allahdadi, F.A. (1993). High strain lagrangian hydrodynamics: A Three-Dimensional SPH Code for Dynamic Material Response. *Journal of Computational Physics*. **109:1**, 37-75.

Gray, J.P., Monaghan, J.J. and Swift, R.P. (2001). SPH elastic dynamics. *Computer Methods in Applied Mechanics and Engineering*. **190:49**, 6641-6662.

Chen, J.K., Beraun, J.E. and Jih, C.J. (1999). Completeness of corrective smoothed particle method for linear elastodynamics. *Computional Mechanics*. **24**, 273-285.

Liu, G.R. and Liu, M.B. (2003). Smoothed Particle Hydrodynamics. World Scientifice Publishing.

Monaghan, J.J. (1989). On the problem of penetration in particle methods. *Journal of Computational Physics*. **82**, 1-15.

Bui, H.H., Fukagawa, R. and Sako, K. (2010). A Study of the Matter of SPH Application to Saturated Soil Problems. *The 5th international SPHERIC workshop*, 354-361.